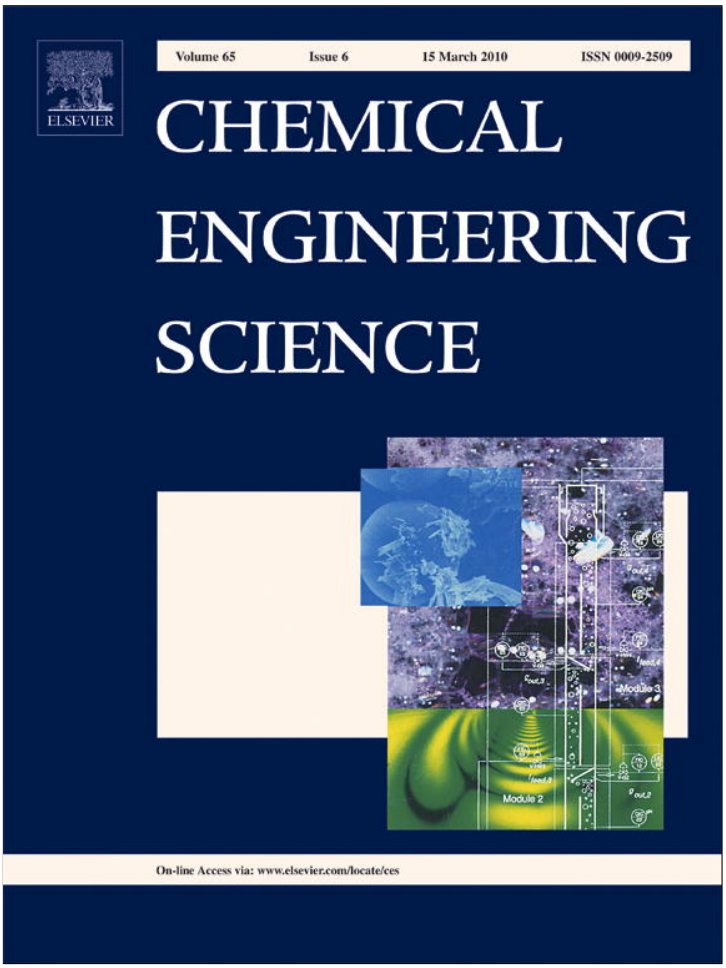

Chemical Engineering Science 65 (2010) 2037–2051

Contents lists available at ScienceDirect

Chemical Engineering Science

journal homepage: www.elsevier.com/locate/ces

Validated simulation of droplet sedimentation with finite-element and level-set methods

Evangelos Bertakis [a], Sven Groß [b], Jörg Grande [b], Oliver Fortmeier [c], Arnold Reusken [b], Andreas Pfennig [a,*]

[a] AVT—Thermal Process Engineering, RWTH Aachen University, Wüllnerstrasse 5, D-52056 Aachen, Germany
[b] Numerical Mathematics, RWTH Aachen University, Templergraben 55, D-52056 Aachen, Germany
[c] Scientific Computing, RWTH Aachen University, Seffenter Weg 23, D-52074 Aachen, Germany

ARTICLE INFO

Article history:
Received 9 February 2009
Received in revised form
3 November 2009
Accepted 25 November 2009
Available online 3 December 2009

Keywords:
Drop
Extraction
Hydrodynamics
Interface
Sedimentation
Dynamic simulation

ABSTRACT

In the present paper freely sedimenting *n*-butanol droplets in water are simulated by means of computational fluid dynamics. The finite-element and the extended finite-element methods were implemented and evaluated. The level-set function is used for capturing the interface movement. The three-dimensional nonstationary simulations included the stages of droplet acceleration, deformation, and stability in terms of shape and velocity. The influence of the grid resolution, the computational domain walls, and the droplet initial velocity was investigated and quantified. The droplet diameters that were studied spanned the region of spherical, deformed, and oscillating droplets. The simulation results were compared to experiments and empirical models in terms of droplet shape, oscillation behavior and terminal velocity, showing good agreement. The extended finite-element method was found to provide simulation results in better accordance to the experiments and empirical models than the conventional finite-element method.

1. Introduction

The development of a predictive model for liquid–liquid extraction columns demands detailed study of single droplets. The most important parameters that need to be investigated are the mass transfer properties between the two phases and the droplet sedimentation velocity (Henschke and Pfennig, 1999). The results of such studies are used for the development of engineering models that describe the whole extraction process where millions of droplets are involved (Henschke, 2003; Kalem and Pfennig, 2007). In order to make the scale-up possible, robust and accurate models are required. Also, considerable experimental effort is needed for the accurate measuring of these data.

Early models for calculating the terminal velocity of droplets moving freely in a liquid continuum assume that the droplet retains a rigid spherical shape. Attempts to take the droplet shape and interfacial mobility into account have produced various semi-empirical formulas and algebraic correlations (Clift et al., 1978; Levich, 1962; Rose and Kintner, 1966). While very small droplets can be realistically modelled as hard spheres, bigger droplets exhibit an internal circulation and, therefore, a mobile interface has to be taken into account. As the terminal velocity increases with droplet size, a critical diameter is reached where the drop gets deformed and flattened and this leads to a higher hydrodynamic resistance. Beyond that diameter, the sedimentation velocity of even bigger oscillating droplets starts to decrease (Hu and Kintner, 1955). In addition, the interfacial tension influences the droplet shape (Feigl et al., 2007) and it is thus important to take the dynamic phenomenon of interfacial movement into account if an accurate model for the simulation of droplet sedimentation is to be developed. E.g., Waheed et al. (2004) conducted two-dimensional axis-symmetrical finite element simulations of a droplet in an uniform counter-current. The droplet was of constant spherical shape and the interface was considered ideally mobile. The sedimentation velocity results for oscillating droplets exhibited inadequate agreement with the experimental data for large droplets, indicating that a predictive method for the sedimentation of single droplets must take a freely deformable interface into account in order to be realistic.

The literature covering the simulation and modelling of bubbles and droplets moving in a liquid medium is vast and a comprehensive review is not the purpose of this article. Results from the literature that are relevant for the topic addressed in this paper are briefly discussed below.

In general, free interfacial movement can be simulated by either "tracking" or "capturing" the interface. In the front-tracking methods, the interface is explicitly represented by additional computational elements that follow its movement.

* Corresponding author. Tel.: +49 241 80 95490; fax: +49 241 80 92332.
E-mail address: andreas.pfennig@avt.rwth-aachen.de (A. Pfennig).

0009-2509/$ - see front matter © 2009 Elsevier Ltd. All rights reserved.
doi:10.1016/j.ces.2009.11.043

This is avoided in the front capturing methods where the position of the interface is represented implicitly using some indicator function. Noteworthy alternative approaches for interface treatment are the "phase field" or "diffuse interface" method and the lattice-Boltzmann technique.

Li and Mao (2001) and Li et al. (2003) as well as Mao et al. (2001) investigated the effect of surfactants on droplets and bubbles based on the front-tracking method introduced originally by Ryskin and Leal (1983). Petera and Weatherley (2001) used a front-tracking method for the two-dimensional axis-symmetrical system of a falling droplet. Their results for the sedimentation velocities are in good agreement with the experiments, but only a small range of dr*a* oplet diameters was investigated in which the droplets are not expected to exhibit strong interfacial movement (Mack, 2001). The "moving grid" front-tracking technique was used by Quan and Schmidt (2006) for the simulation of a liquid droplet in a gaseous current. An implementation of the "marker point" front-tracking method (Cristini et al., 1998, 2001) was compared to experimental results for droplet breakup by Patel et al. (2003).

The two most popular front-capturing methods used are the "level-set" technique and the "volume of fluid" (VOF) method. The VOF method, first presented by Hirt and Nichols (1981), was used by Koebe (2004) to study the behavior of sedimenting bubbles showing promising results. Renardy et al. (2001) implemented the VOF method to simulate droplet deformation and breakup. Gueyffier et al. (1999) compared results obtained with the VOF method to experimental data and algebraic correlations for sedimenting bubbles and droplets showing good agreement.

The level-set function, proposed by Osher and Sethian (1988), was implemented by Sussman et al. (1994) for two-dimensional droplet simulations with a finite interface thickness. Although they report good numerical convergence properties and realistic results for both small droplets with high interfacial tension and big droplets with low interfacial tension, they do not compare their results to experimental data. The level-set function has also been used by Deshpande and Zimmerman (2006) for two-dimensional simulations of mass transfer between sedimenting droplets and continuous phase for low Reynolds numbers ($Re < 3$). Yang and Mao (2005) and consequently Wang et al. (2008) simulated the mass transfer between droplet and continuous phase in two dimensions using the level-set method. The simulation results show good agreement with the experiments, but were limited to droplets with diameter smaller than 2 mm. Pillapakkam and Singh (2001) also performed simulations with the level-set technique for droplets subjected to shear flows and sedimenting bubbles.

A hybrid between the front-capturing and the front-tracking methods is proposed by Tryggvason et al. (2001) and implemented by Muradoglu and Tryggvason (2008) for rising bubbles. The results were compared to experimental data showing good agreement for both pure and surfactant-contaminated systems. In order to combine the advantages and eliminate the weaknesses of the VOF and the level-set methods, it is possible to couple them as shown by Yang et al. (2006) and Sussman et al. (2007). In the latter article there is also a comparison of the simulation results with experimental data for rising bubbles exhibiting good accuracy.

Amongst the experimental approaches to the problem, Wegener et al. (2007a) measured the velocity of buoyancy-driven toluene droplets rising in an aqueous continuum as a function of time. The corresponding numerical investigations (Wegener et al., 2007b), however, assume a spherical droplet of constant shape and were constrained to a single droplet diameter. Dehkordi et al. (2007) studied the sedimentation of *n*-butanol droplets under mass transfer conditions with and without surfactants. Alves et al. (2005) applied the stagnant-cap model on experimentally obtained terminal velocity values of air bubbles rising in water in order to take the effect of bubble contamination on rise velocity and mass transfer into account. Large droplets that are important in engineering applications were studied experimentally by various authors (Hendrix et al., 1967; Mekasut et al., 1979; Steiner et al., 1990). Based on the experimental results these papers also treat modelling issues. Early experimental investigations concerning the shape of rising droplets and a qualitative comparison to numerical calculations was performed by Koh and Leal (1990) as well as by Noh et al. (1993).

Although some of the aforementioned works do include qualitative or even quantitative comparisons of the simulations to experimental data, these are rather limited (e.g., only two-dimensional simulations; only small droplets). To our knowledge there is no study in the literature where the sedimentation velocity of a real liquid–liquid extraction system is accurately simulated with a freely movable interface for a wide spectrum of droplet diameters that also covers the oscillating region. Furthermore, a systematic comparison to experimental results is necessary in order to establish the numerical technique as trustworthy for engineering applications. The focus of this study is to fill this gap, thus establishing a solid simulation tool in which models that describe other single-droplet phenomena, like mass transfer and surfactant influence, can be safely implemented.

2. Experimental investigations

For the sedimentation velocity measurements a standard sedimentation apparatus is used (Henschke, 2003; Gross-Hardt et al., 2002). A drawing of the sedimentation apparatus can be seen in Fig. 1. The droplets are generated through a nozzle submerged in a cylindrical cell that contains the continuous phase. The droplet generation was controlled by a Hamilton "Microlab M" syringe dosimetry pump. The droplet size was determined by the liquid volume discharged by the pump that was set as a free variable. Thus, from the known droplet volume the diameter of the respective sphere was calculated, that is used in this work to express droplet size. For each drop volume the nozzle was chosen from a set of nozzles with different inner

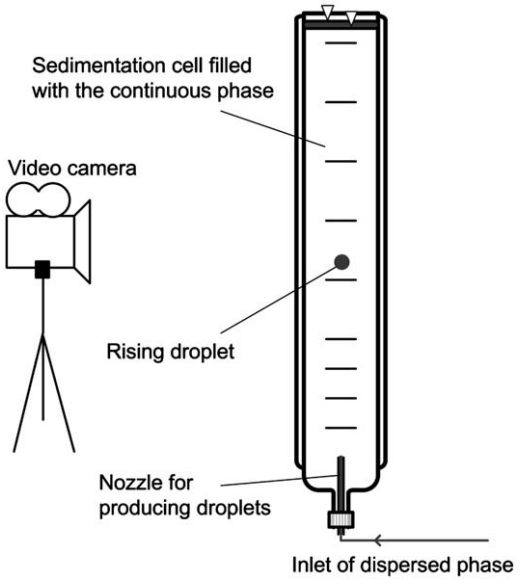

Fig. 1. Drawing of experimental setup.

diameters such that clean detachment of the drop from the tip of the nozzle was achieved.

The cell is 40 mm in diameter and 500 mm in height and has a marked measuring region 100 mm in length. Upon generation, the droplet is given about 12 cm acceleration distance in order to reach its terminal velocity and its position is monitored using a camera recording 30 frames per second. The amount of frames recorded from the time the droplet enters the measuring region to the time of exit, delivers the droplet travel time for the given distance. From these data the terminal rise velocity of the droplet is calculated (Paesch, 1998). For every droplet diameter two series of measurements were performed. In each of the two series, 20 droplets were generated separated by 3 s time-intervals. The average amount of frames of all droplets is used to calculate the sedimentation velocity for that diameter. In a batch of 20 droplets, the maximum deviation of a single measurement from the average was found to be no greater than 3 frames, i.e. 0.1 s, whereas the maximum deviation between two measurements was no greater than 4 frames. The averages of the two series were also in good agreement, presenting a deviation of maximum 1 frame.

The measuring cell and the nozzle were cleaned using chromosulfuric acid, and then washed with bidistilled water and acetone. The dosimetry syringe, as well as the PTFE tubings that were used, were cleaned with acetone and then dried. An additional washing step was performed using the same organic solvent that was also used in the dispersed phase.

In this paper, the solvent extraction standard-test system of *n*-butanol droplets sedimenting in water is considered (Misek et al., 1985). The physicochemical data of the mutually saturated continuous and dispersed phase are given in Table 1. The water used was deionized and bidistilled. The *n*-butanol was of analytical grade provided by Merck Germany. The temperature of the measurements was 293 ± 0.5 K. The droplet diameters range in the experiments from 1.56 to 3.48 mm. The measurement error of the droplet terminal velocity increases as the sedimentation speed rises. The relative errors in this work vary from 1.5% for the slowest droplet to 2.1% for the fastest one. The experimental error in determining the droplet diameter decreases as the droplet volume increases. The droplet diameter error in this work varies from ± 0.1 mm for the smallest droplet to ± 0.05 mm for the biggest one.

3. Evaluation with semi-empirical models

For the validation of the experimental as well as the simulation results two empirical criteria are used, as well as one semi-empirical model. The purpose of these comparisons is to evaluate the agreement of the measured and the calculated data to the existing models and experimental observations. The two empirical criteria provide qualitative information as to the droplet shape and mobility. The semi-empirical model describes the droplet sedimentation velocity as a function of material data alone, thus providing a quantitative measure of the simulation result validity.

Table 1
Physicochemical data of the mutually saturated phases of *n*-butanol and water.

Property	Phase	
	Aqueous	Organic
Density (kg/m^3)	986.51	845.44
Viscosity μ (10^{-3} Pa s)	1.39	3.28
Interfacial tension σ (mN/m)	1.63	

The first criterion was presented by Clift et al. (1978) and consists of a diagram correlating the shape of droplets rising or falling freely in infinite media to the Reynolds (*Re*), Eötvös (*Eo*), and Morton (*Mo*) numbers:

$$Re = \frac{v_{sed} d \rho_c}{\mu_c} \tag{1}$$

$$Eo = \frac{d^2 g \Delta\rho}{\sigma} \tag{2}$$

$$Mo = \frac{\mu_c^4 g \Delta\rho}{\rho_c^2 \sigma^3} \tag{3}$$

$$\Delta\rho = |\rho_c - \rho_d| \tag{4}$$

where d is the droplet diameter, v_{sed} is the droplet sedimentation velocity, ρ is the density, μ is the dynamic viscosity, σ is the interfacial tension, g is the gravitational acceleration and the subscripts c and d indicate the continuous and the dispersed phase, respectively. The Reynolds and Eötvös numbers are used to correlate the droplet shape with droplet characteristics like sedimentation velocity and diameter. The Morton number is independent of these droplet characteristics, and is therefore constant for the given binary material system. In this work the Morton number equals $Mo = 1.22 \times 10^{-6}$, and according to Clift et al. (1978), droplets with $Re < 25$, $Eo < 0.8$ and thus $d \leq 1.0$ mm, are expected to be spherical, whereas droplets beyond these limits are expected to be ellipsoidal. The diagram of Clift et al. (1978) is considered a standard reference for predicting the shape of fluid particles, and has been found to agree well with CFD simulations also by other authors (Smolianski, 2005).

The second criterion is described by Mack (2001) and is used to categorize the droplets according to their diameter in rigid, circulating, or oscillating droplets. The categorization is performed according to the following relations:

$$\text{circulating droplets}: \quad \frac{1.83}{Mo^{0.275}} \leq Ar \leq \frac{391}{Mo^{0.275}} \tag{5}$$

$$\text{oscillating droplets}: \quad \frac{391}{Mo^{0.275}} \leq Ar \leq \frac{1.31 \times 10^4}{Mo^{0.275}} \tag{6}$$

$$Ar = \frac{d^3 g \rho_c \Delta\rho}{\mu_c^2} \tag{7}$$

Ar is the Archimedes number, which in the experiments in this paper ranges from 2690 to 29 864. From these equations, the droplet state can be predicted depending on the droplet diameter. For the system used in this work it is found that droplets with $0.48 \text{ mm} \leq d \leq 2.85$ mm according to this criterion should have an internal circulation. Smaller droplets are rigid and spherical, whereas bigger droplets exhibit an oscillating behavior.

Henschke (2003) derived a set of model equations for scale-up calculations of extraction columns that allows the droplet sedimentation velocity to be described as a function of droplet diameter that is continuous over the whole diameter range. The model is based on the physicochemical properties of the system and contains three adjustable parameters that can be fitted to experimental data.

In the derivation of this model, existing equations, like those found e.g. in Brauer (1973) and Modigell (1981), were compared to experimental data and improved with the help of two-dimensional CFD simulations (Haas et al., 1972; Henschke et al., 2000; Waheed, 2001). The new correlated equations were valid for spherical droplets with either a rigid or an ideally mobile interface. The sedimentation velocity of indented and oscillating droplets was calculated according to Clift et al. (1978) and Maneri (1995), respectively. Additional equations and parameters were

used to describe the transitions between the regions of rigid, circulating, indented, and oscillating droplets, as well as to combine all the equations in a continuous function.

The Reynolds number of spherical droplets with a rigid interface that do not exhibit an internal circulation is calculated by the following equations (Henschke et al., 2000):

$$Re_{rigid} = \sqrt{\frac{4Ar}{3C_{D,rigid}}} \tag{8}$$

$$C_{D,rigid} = \frac{432}{Ar} + \frac{20}{Ar^{1/3}} + 0.51\frac{Ar^{1/3}}{Ar^{1/3}+140} \tag{9}$$

where $C_{D,rigid}$ is the drag coefficient of the droplet. The Reynolds number of spherical droplets with an ideally mobile interface, and therefore an ideal internal circulation, is calculated from the following equation:

$$Re_{circ} = \frac{Ar}{12(0.065Ar+1)^{1/6}} \tag{10}$$

For taking into account the extent of interfacial mobility, and thus the transition from rigid to ideally circulating spherical droplets, the Hadamard–Rybczynski factor K_{HR} (Levich, 1962) was corrected using the following equation:

$$f_{circ} = 1 - \frac{1}{1+(d/p_1)^{10}} \tag{11}$$

that includes parameter p_1 of the model to represent this transition. The corrected Hadamard–Rybczynski factor K'_{HR} is calculated as

$$K'_{HR} = \frac{3(\mu_c+\mu_d/f_{circ})}{2\mu_c+3\mu_d/f_{circ}} \tag{12}$$

The Reynolds number of spherical droplets in between the two boundary states of rigid and ideally circulating interface is given by

$$Re_{shpere} = (1-f'_{circ})Re_{rigid} + f'_{circ}\,Re_{circ} \tag{13}$$

$$f'_{circ} = 2(K'_{HR}-1) \tag{14}$$

Thus, the terminal velocity of spherical droplets, that is corrected according to their interfacial mobility, is given by

$$v_{sphere} = \frac{\mu_c Re_{sphere}}{d\rho_c} \tag{15}$$

The velocity of deformed droplets is calculated by the empirical equation

$$v_{def} = \sqrt{\frac{dg\Delta\rho}{2\rho_c}} \tag{16}$$

Likewise, for oscillating droplets, the equation used is

$$v_{os} = \sqrt{\frac{2p_2\sigma}{d\rho_c}} \tag{17}$$

where parameter p_2 of the model is used to determine the velocity of droplets in that region. At this point, it is interesting to note that the velocity of deformed droplets increases with increasing droplet diameter, while the velocity of oscillating droplets decreases with increasing droplet diameter. The transition from oscillating to deformed droplets is expressed through the combination of the two respective velocities:

$$v_{def,os} = (v_{def}^{\alpha} + v_{os}^{\alpha})^{1/\alpha} \tag{18}$$

where $\alpha = 8$ was chosen empirically in previous work (Henschke, 2003). Finally, the sedimentation velocity of the droplet is calculated by combining the velocities of spherical, deformed, and oscillating droplets in the equation:

$$v_{sed} = \frac{v_{def,os}v_{sphere}}{(v_{def,os}^{p_3} + v_{sphere}^{p_3})^{1/p_3}} \tag{19}$$

that includes parameter p_3 of the model that represents the transition from the viscous force dominated region to the surface force dominated region with increasing droplet diameter.

As an alternative to fitting the first parameter to experimental data, it can be set to a value tending either to zero or to infinity. The curves that are obtained for these two boundary values represent the behavior of droplets with either an ideally mobile or a rigid interface, respectively. For a system free of surface-active impurities, that can have a significant effect on interface mobility and droplet shape, the CFD-implementation of a free surface model like the level-set function, should provide results that come close to the model curve representing the ideally mobile droplet interface.

In Fig. 2 the model fit to the experimental data is shown together with the model lines representing the ideally mobile and the rigid droplet interface. The fitted values of the parameters were $p_1 = 1.63$ mm, $p_2 = 3.76$, and $p_3 = 2.98$, and, as can be seen in Fig. 2, the model presents a good fit to the experimental data. Model parameter p_1 influences the initial slope of the curve for small diameters, representing the change from rigid to circulating droplets. The shape of the sedimentation curve peak is influenced by parameter p_3 that represents the change from circulating to oscillating droplets. The vertical position of the plateau after the peak is influenced by parameter p_2. Vertical lines indicate the different regions of rigid droplets, circulating droplets and oscillating droplets according to relations (5) and (6). The vertical line separating the regions of circulating and oscillating droplets almost coincides with the peak of the model curve that is fitted to the experimental data. This fact indicates the agreement between the experiments and the empirical criterion presented above (Mack, 2001) as to where the hydrodynamic resistance due to droplet deformation becomes more significant than the buoyancy force, thus leading to a decay of sedimentation velocity with increasing droplet size. The experimental results are included in the data summary given in Table 2.

4. Numerical simulation

For the numerical simulation of the sedimenting droplet the custom-made three-dimensional finite element package DROPS (Gross et al., 2002, 2006) is used. The code is written in C++ and is also used in other applications such as heat transfer and flow problems in falling films (Gross et al., 2005). In Sections 4.1 and 4.2 some of the numerical methods and modules implemented in DROPS are briefly discussed. For a more detailed description see Gross et al. (2006) and the DROPS internet homepage (Reusken et al., 2009). As the simulation of three-dimensional two-phase flow problems has a very high numerical complexity, most parts of the code have been parallelized. A few parallelization issues are addressed in Section 4.4.

4.1. Model for two-phase flows

For the modelling of a two-phase droplet problem the two phases Ω_1 (droplet) and Ω_2 (continuous phase) are assumed to behave like incompressible immiscible Newtonian fluids. Conservation of mass and momentum yields the incompressible Navier–Stokes equations in each phase with a free boundary condition at the interface $\Gamma = \Gamma(t) = \partial\Omega_1$, where the standard assumption is made, that surface tension balances the jump of the normal stress on the interface and the normal and tangential

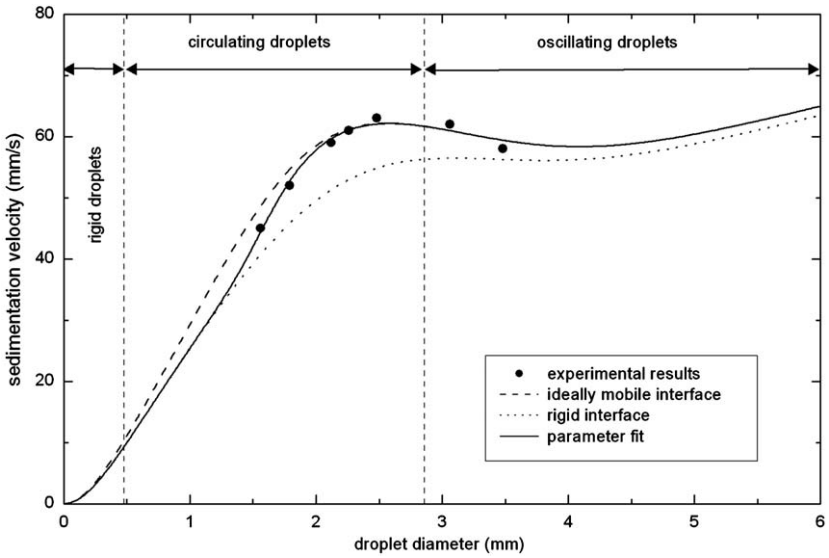

Fig. 2. Experimental data and sedimentation curves of the Henschke (2003) model.

Table 2
Sedimentation velocities and dimensionless numbers for all studied *n*-butanol droplets in continuous water phase.

d (mm)	v_{sed} (mm/s)	Re	Eo	Ar
1.0 (*)	27.6	19.6	0.85	709
1.5 (*)	44	46.9	1.91	2392
1.56	45	49.9	2.07	2690
1.79	52	66.2	2.72	4064
2.0 (*)	57	81.0	3.40	5669
2.12	59	88.9	3.82	6752
2.26	61	98.0	4.34	8180
2.48	63	111.0	5.22	10 808
3.0 (*)	60	127.9	7.64	19 132
3.06	62	134.8	7.95	20 303
3.48	58	143.5	10.3	29 864
4.0 (*)	55	156.4	13.6	45 351

The asterisk (*) is used to denote the simulated data.

velocities are continuous at the interface, i.e.,

$$[\boldsymbol{\sigma}\cdot\mathbf{n}]_\Gamma = \sigma\kappa\mathbf{n}, \quad [\mathbf{u}]_\Gamma = 0$$

Here $\mathbf{n}=\mathbf{n}_\Gamma$ is the unit normal at the interface (pointing from Ω_1 in Ω_2), σ the surface tension coefficient, κ the curvature of Γ and $\boldsymbol{\sigma}$ the stress tensor, i.e.,

$$\boldsymbol{\sigma} = -p\mathbf{I}+\mu\mathbf{D}(\mathbf{u}), \quad \mathbf{D}(\mathbf{u}) = \nabla\mathbf{u}+(\nabla\mathbf{u})^T$$

with $p=p(x,t)$ the pressure, $\mathbf{u}=\mathbf{u}(x,t)$ the velocity vector and μ the dynamic viscosity.

This model for a two-phase incompressible flow problem is often used in the literature. The effect of the surface tension can be expressed in terms of a localized force at the interface, cf. the so-called "continuum surface force" (CSF) model (Brackbill et al., 1992; Chang et al., 1996). This localized force is given by

$$f_\Gamma = \sigma\kappa\delta_\Gamma\mathbf{n}_\Gamma$$

Here δ_Γ is a Dirac δ- function with support on Γ. This localization approach can be combined with the level-set method for capturing the unknown interface. Here the main idea is outlined, for a detailed treatment see Chang et al. (1996). The level-set function, denoted by $\phi=\phi(x,t)$, is a scalar function with $\phi(x,t)<0$ for $x\in\Omega_1(t)$, $\phi(x,t)>0$ for $x\in\Omega_2(t)$ and $\phi(x,t)=0$ for $x\in\Gamma(t)$. Hence, the interface is implicitly given by the zero-level of the level-set function. For the advection of the interface the linear hyperbolic level-set equation $\phi_t+\mathbf{u}\cdot\nabla\phi=0$ for $t\geq 0$ and $x\in\Omega$ is introduced. The jumps in the coefficients ρ and μ can be described using the level-set function in combination with the discontinuous Heaviside function H

$$\rho(\phi) := \rho_1+(\rho_2-\rho_1)H(\phi)$$

$$\mu(\phi) := \mu_1+(\mu_2-\mu_1)H(\phi) \tag{20}$$

where $H(\phi)=0$ for $\phi<0$ and $H(\phi)=1$ for $\phi>0$. Combination of the CSF approach with the level-set method leads to the following model for the two-phase problem in $\Omega\times[0,T]$:

$$\rho(\phi)\left(\frac{\partial\mathbf{u}}{\partial t}+(\mathbf{u}\cdot\nabla)\mathbf{u}\right) = -\nabla p+\rho(\phi)\mathbf{g}+\mathrm{div}(\mu(\phi)\mathbf{D}(\mathbf{u}))+\sigma\kappa\delta_\Gamma\mathbf{n}_\Gamma \tag{21}$$

$$\mathrm{div}\,\mathbf{u} = 0 \tag{22}$$

$$\phi_t+\mathbf{u}\cdot\nabla\phi = 0 \tag{23}$$

together with suitable initial and boundary conditions for $\mathbf{u}$ and ϕ. This is the continuous problem that is used to model the two-phase problem. It is also used in, for example, Chang et al. (1996), Pillapakkam and Singh (2001), Sussman et al. (1999) and Tornberg and Engquist (2000).

Relying only on the advection equation (23) for the evolution of the level set function is not enough, since it would degenerate over time. This affects the treatment of the discontinuities and the refinement of the interfacial region. To avoid this undesirable behavior a reparametrization scheme for the level-set function was implemented such that ϕ remains close to a signed distance function. Moreover, this reparametrization is used to smooth the level-set function close to the interface and thus stabilize its evolution. A common problem with the level-set function is that mass conservation is not inherently included in the formulation. In general the volume of the droplet will shrink with time. This numerical loss of volume, however, reduces if a finer grid is used. An interface shift is applied to compensate for the volume loss (Gross et al., 2006). An alternative approach for obtaining better mass conservation, based on a suitable source term in the transport equation for ϕ, is given in Zimmerman (2006).

4.2. Discretization

The spatial discretization is based on a multilevel hierarchy of tetrahedral grids. The initial tetrahedral triangulation of the computational domain Ω used in the simulations is shown in Fig. 3, where the initial droplet position can also be seen. An adaptive refinement algorithm (Gross and Reusken, 2005) has been implemented which allows for a high grid resolution close to the interface where most of the interesting phenomena occur. As time evolves the grid is updated by refinement and coarsening to adapt it to the new position of the drop, cf. Fig. 4.

At the initialization of the simulation, the droplet is centrally placed slightly above the bottom of an orthogonal computational domain. The domain dimensions were set depending on the droplet diameter so that the walls are at a relatively safe distance from the droplet interface (see Section 5.1.5 for a discussion on the issue). A no-slip boundary condition is applied on the domain wall. Depending on the droplet diameter, the domain height is chosen such that during the simulation the droplet moves approximately through half the domain height. Due to this, the effect of the upper domain wall can be neglected. The mesh size close to the droplet interface is gradually decreased. The mesh size in the vicinity of the interface is directly related to the number of (local) refinement levels. In a refinement step a marked tetrahedron is divided into eight new elements. In a subsequent grid closure step "hanging nodes" are eliminated. The refinement algorithm is such that the hierarchy of tetrahedral triangulations is stable, i.e., strongly deteriorated tetrahedra with very small angles do not occur. The range around the droplet interface where the local refinement is applied is set using a simulation parameter. In our applications this parameter has a value of approximately the droplet radius. In the discussion below the grid resolution is characterized by the mesh size of the elements close to the droplet interface. The number of refinement levels has a considerable impact on the simulation's duration. Using an AMD Athlon 64 X2 4200+CPU with 3 GB of memory, the time needed to perform the simulations presented in this work ranged from 2 days for simulations with relatively coarse grids and small domains, to 5 days for simulations with fine grids and large domains. During the simulation, the droplet speed was monitored, and the simulation was run until the droplet reached a state where either the rise velocity was constant, or it constantly oscillated around a stable value (as presented in Section 5).

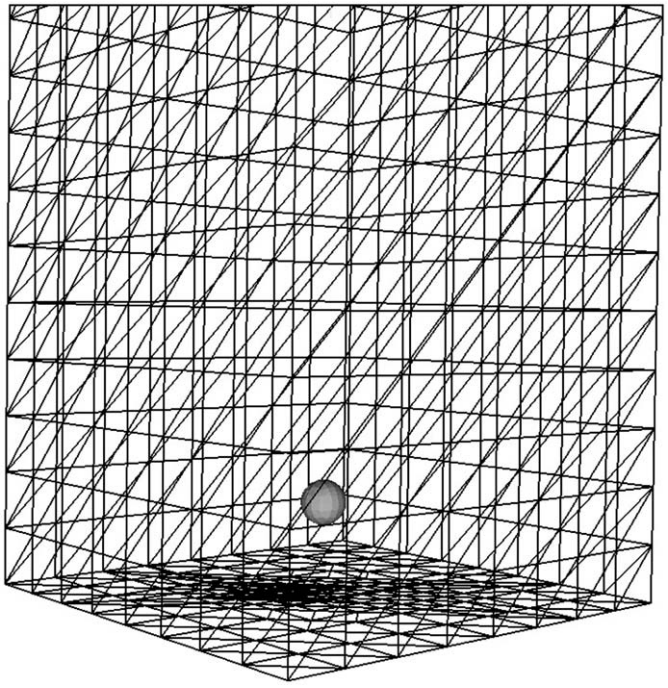

Fig. 3. Computational domain and initial grid for a droplet with diameter of 1.0 mm.

For discretization of the flow variables and of the level-set function a finite-element approach is used (Gross et al., 2002). For the spatial discretization of the velocity $\mathbf{u}$ and pressure p the LBB-stable Hood–Taylor P_2-P_1 finite-element pair is used. The level-set function ϕ is discretized by continuous piecewise quadratic finite elements. The finite-element method for the level-set advection equation (23) is stabilized by a standard streamline diffusion technique (Roos et al., 1996).

For the finite element discretization of the Navier–Stokes equations, integrals over tetrahedra T have to be evaluated, having discontinuous integrands (due to ρ, μ) if T is cut by Γ. Note that in such a case we do not apply any smoothing (e.g., by replacing H in Eq. (20) by a smoothed Heaviside function H_ε), but integrate over the parts $\Omega_i \cap T$, $i=1,2$, where the integrands are continuous and thus standard quadrature rules can be applied. Thus our approach is a "sharp interface method". For this one needs an approximation Γ_h of the zero level of the level set function ϕ. This approximation is constructed by replacing the piecewise quadratic finite element approximation ϕ_h of ϕ by a piecewise linear function $\tilde{\phi}_h$ on a refined mesh (ϕ_h and $\tilde{\phi}_h$ have the same values at all vertices of the refined mesh). The piecewise planar zero level of $\tilde{\phi}_h$, which can easily be determined, yields the approximate interface Γ_h.

For the numerical treatment of the surface force term f_Γ a modified Laplace–Beltrami technique is applied to avoid an explicit computation of the curvature which would involve the approximate evaluation of second order derivatives. As the force is only localized at the interface Γ, its weak formulation is evaluated as a surface integral on Γ_h. More details concerning the interface approximation and discretization of the surface-force term can be found in Gross and Reusken (2007b).

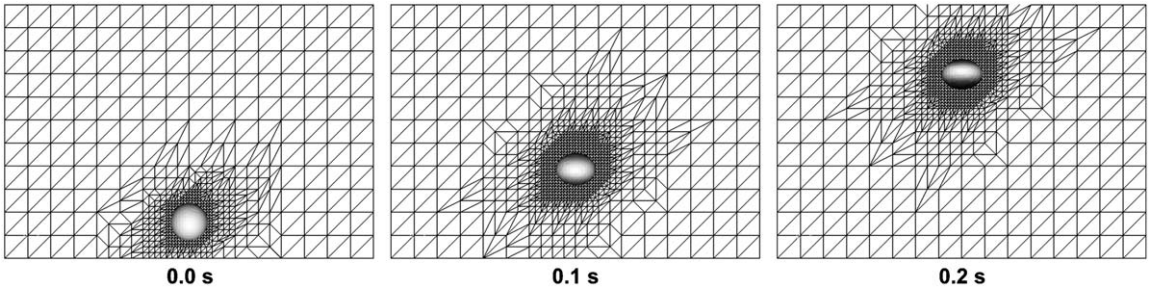

Fig. 4. Evolution of the grid with droplet movement.

For the numerical time integration the fractional step θ-scheme (Bristeau et al., 1987) is applied. This method has second order accuracy and is strongly A-stable. In each time step a quasi-stationary coupled system of Navier–Stokes and level-set equations has to be solved. This coupling and the nonlinearity of the Navier–Stokes problem are treated by an outer Picard iteration. The remaining linear Oseen problems are solved by a preconditioned Krylov subspace solver (GCR) or an inexact Uzawa iteration. For the preconditioning of the diffusive part of the operator Krylov subspace methods or multigrid solvers are used. The level-set equation is solved by a preconditioned GMRES solver.

4.3. The XFEM space

In actual engineering applications of liquid–liquid droplet dispersions, often the surface tension is a driving force for the flow problem. In such cases there is a relatively high pressure jump across the interface.

The interface, which is implicitly given by the zero level of the level-set function, is in general not aligned with the triangulation that is used in the discretization of the flow problem. This non-alignment causes severe difficulties with respect to the discretization of the localized surface-tension force and the discretization of the pressure variable, which is *discontinuous* across the interface. In standard finite-element spaces the functions used for discretization are either continuous or discontinuous across element borders, but in general (due to non-alignment) *continuous across the interface*, and thus not very suitable for the approximation of the discontinuous pressure. In many simulations these effects cause strong unphysical oscillations of the velocity vector at the interface, the so-called "spurious velocities". These spurious velocities can be avoided to a large extent if in addition to the modified Laplace–Beltrami discretization that is used for the surface tension force, an "extended finite-element" (XFEM) space is implemented for the discretization of the pressure.

For the construction of the XFEM space we first consider the standard finite element space Q_h of piecewise linear functions and $q_1, \ldots, q_n \in Q_h$ its nodal basis functions with $n := \dim Q_h$. Let $\mathcal{I}_\Gamma \subset \{1, \ldots, n\}$ be the set of indices associated to the tetrahedra intersected by Γ. For each of these indices $i \in \mathcal{I}_\Gamma$, an additional basis function q_i^Γ is introduced which is discontinuous at the interface:

$$q_i^\Gamma(\mathbf{x}) := q_i(\mathbf{x}) \cdot (H_\Gamma(\mathbf{x}) - H_\Gamma(\mathbf{x}_i)), \quad \mathbf{x} \in \Omega$$

with $H_\Gamma(\mathbf{x}) = 0$ for $\mathbf{x} \in \Omega_1$ and $H_\Gamma(\mathbf{x}) = 1$ for $\mathbf{x} \in \Omega_2$. Then the pressure XFEM space Q_h^Γ is defined by the span of $\{q_i\}_{i=1}^n \cup \{q_i^\Gamma\}_{i \in \mathcal{I}_\Gamma}$. Hence, the XFEM space consists of all functions which are piecewise linear on each of the subdomains Ω_1, Ω_2, respectively, but may have a jump across the interface. This favorable property can be seen in Fig. 5, where the approximations of the pressure jump of a static droplet due to surface tension is shown for the standard FEM space Q_h and the XFEM space Q_h^Γ. The XFEM approach was originally introduced and applied to fracture mechanics in Moës et al. (1999), a related work is Hansbo and Hansbo (2004). For more details regarding the pressure XFEM space for two-phase flow problems see Gross and Reusken (2007a) and Reusken (2008).

In this paper, two versions of the DROPS CFD-package are considered: one based on the standard finite-element space (P_2-P_1) and one using the new XFEM approach for the pressure variable.

4.4. Parallelization

To achieve a higher accuracy with a DROPS simulation, the computational grid can be locally refined in the domain of interest, i.e. close to the interface. Still for three-dimensional simulations with a high grid resolution the storage requirements and computation time may easily exceed the capacity of a serial processor. For being able to handle such big computational problems in an acceptable time, the computations must be done on a high performance computer. A shared memory parallelization with OpenMP has been implemented, see Terboven et al. (2005) for results. Another strategy is to use multiple processes, where "process" means a computing unit with its own memory (called "distributed memory"). A distributed-memory parallelization of DROPS is under development using MPI (Walker and Dongarra, 1996) to handle the communication and synchronization of processes. This parallelization applies the following domain decomposition approach. Applying a suitable load balancing strategy, the tetrahedra of the finest level of the grid hierarchy are distributed among the processors resulting also in a distribution of the velocity, pressure and level-set unknowns. After grid refinement/coarsening a load redistribution is performed. The standard finite-element (P_2-P_1) discretization of the Navier–Stokes equations and of the level-set equation have an inherent data locality property and thus are relatively easy to parallelize. For solving the discrete systems, parallel preconditioned Krylov subspace methods are implemented. The parallel iterative methods use techniques for reducing the number of synchronization points in each iteration. Unfortunately, a parallel implementation of the XFEM-discretization is not available, yet. Compared to the standard finite-element method this method is more difficult to parallelize since the extended finite-element space changes depending on the dynamics of the interface. Since this XFEM method turns out to be very important for accurate numerical simulations (as is shown in Section 5) the numerical simulations were performed on a serial computer.

5. Numerical experiments for code validation

In this section the influence of the simulation parameters like mesh size and computational domain size are discussed. The

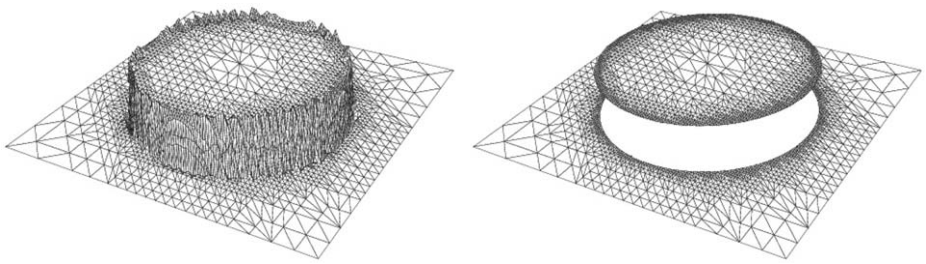

Fig. 5. Finite element approximation of pressure jump: left $p_h \in Q_h$ (standard FEM), right $p_h \in Q_h^\Gamma$ (XFEM).

findings are used in order to discriminate amongst the calculations those that provide the most valid results. The results of these simulations are then evaluated according to the three criteria discussed in Section 3. The simulation results are realized as the calculated droplet position for every simulation time step, from which the corresponding droplet velocities can be calculated by numerical differentiation. If these velocities are plotted versus time, a velocity plateau is eventually reached that indicates the steady-state sedimentation velocity (v_{sed}) for the given configuration.

The droplet diameters considered in this work range from 1 to 4 mm. The *Re*, *Eo* and *Ar* numbers for all the droplets studied, both experimentally and numerically, can be seen in Table 2. In Fig. 6 the shapes of droplets with different diameters are displayed as a function of time. The results are in qualitative agreement with the empirical correlations discussed in Section 3. The smallest droplet with $d=1$ mm exhibits a constant spherical shape, whereas slightly bigger droplets of $d=1.5$ and 2.0 mm obtain an ellipsoidal form. Larger droplets of $d=3$ and 4 mm at their steady state are flat and oblate, while they undergo significant changes in shape before they reach their stable form. The droplet with a diameter of $d=4$ mm strongly oscillates at the beginning of the simulation before the steady state is reached. In the case of $d=3$ mm the respective oscillation was not as strong as for $d=4$ mm, but in Fig. 6 it can be seen that the $d=3$ mm droplet also obtains a non-ellipsoidal shape for a short time period. This is in accordance to the second validity criterion that is discussed in Section 3, where it is stated that droplets with $d\leq 1.0$ mm are expected to be spherical and droplets with $d>2.85$ mm are expected to oscillate. When the droplet has reached its terminal velocity, oscillations were not directly visible, but examination of the velocity data as shown in Sections 5.1.4 and 5.1.5 shows that velocity oscillations exist, but have a very short time period.

5.1. Simulation parameters

The simulation parameters that have an important impact on the obtained results are the mesh size, the step size of the time discretization, the initial conditions of the simulation system and the distance between the wall of the computational domain and the droplet interface. A comparison of the DROPS version with standard finite-elements and the DROPS-XFEM version is also presented in this section. The results are compared to the model of Henschke (2003) that was presented in Section 3, and specifically to the sedimentation curve of droplets with an ideally mobile interface. The numerical values of that curve for droplet diameters of $d=1.0$, 2.0, 3.0, and 4.0 mm are $v_{sed}=0.029$, 0.058, 0.061, and 0.058 m/s, respectively. In Figs. 10–13 that follow, these values are being indicated by solid horizontal lines. Thus, the convergence of the simulation results to the corresponding model values for varying simulation parameters can be checked.

5.1.1. Time step

The timestep is a parameter that can have a considerable impact, not only on the generated results and algorithm stability, but also on the simulation duration. In this work two different timesteps are tested, one is 10^{-4} s, and the other 5.0×10^{-4} s. In Fig. 7 (left) the results obtained with the two time steps are shown, where it is seen that both velocity plots are slightly scattered. This scatter is an effect of the numerical differentiation of the droplet position data. Moreover, periodic scatter of high frequency is introduced by the reparametrization of the level-set function. To eliminate the scattering, and to thus increase the accuracy of the calculated droplet terminal velocity, a central moving average smoothing scheme was applied to all subsequent data. The averaging period was equal to the level-set reparametrization period, i.e. 10 time steps. Thus, the averaging scheme acts as a low-pass filter that eliminates the numerical high-frequency scatter in favor of the physical low-frequency effects. The results are shown in Fig. 7 (right), where it can be seen that the curve with the smaller timestep lies above the curve with the larger timestep, but the difference is not significant. The average deviation along the whole curve was found to be 1.9%, while the average deviation at the velocity plateau was 1.5%. Therefore, it is concluded that the obtained results can be considered equivalent for terminal velocity calculations. Thus, the larger step size is used in the following simulations.

5.1.2. Initial velocity

Concerning the droplet velocity at the beginning of the simulation, two possibilities have been tested. In one case the

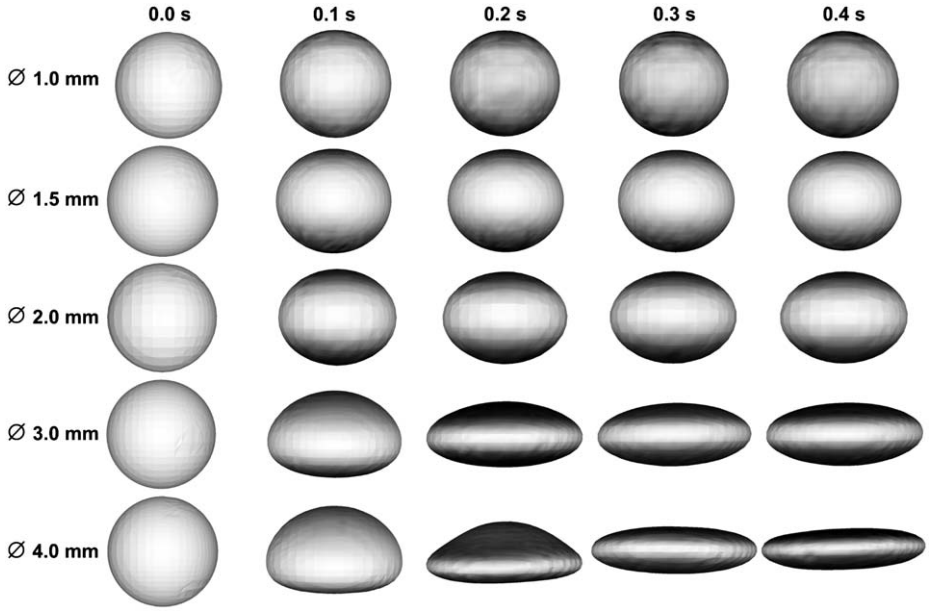

Fig. 6. Comparison of droplet deformation at different time stages for various droplet diameters. All simulations were performed with $v_{init}=0$.

droplet initial velocity is set to zero, and therefore the droplet accelerates to its terminal state. In the second case the droplet is given an initial velocity that is equal to the one predicted from the Stokes' law for the given system and droplet diameter. In this case the droplet is decelerated to its terminal velocity. In Fig. 8 the dependency of the simulation results on the initial velocity of a droplet with a $d = 2.0$ mm diameter are shown. On the left are the results of the plain DROPS version, and on the right are the results of the DROPS-XFEM version. Both droplet velocity curves in each diagram converge to the same terminal sedimentation velocity at the same point in time, independent of the initial conditions. Therefore, the initial droplet velocity has no influence on the obtained final result.

Note that the droplet terminal velocity obtained by the DROPS-XFEM version is slightly higher than the velocity obtained by the plain DROPS version. The deviation of the droplet terminal velocity between the two diagrams of Fig. 8 was found to be 6.8%. This fact is further investigated in Section 5.1.3, where also a finer grid is used to ascertain that this result is grid-independent.

For large droplets ($d \geq 3$ mm) a large initial velocity resulted in droplet breakup, and therefore the droplet sedimentation velocity could not be determined. The pattern of droplet breakup in the simulations resembles those described by Wang and Wang (2007) for large fluid particles where the droplet obtains a bell-like form. In Fig. 9 the simulated droplet breakup stages can be seen. The breakup initializes from the top of the droplet, thus resulting in a torus-like formation, and eventually the droplet breaks up forming two daughter droplets. At this point it is important to note that the volume conservation method mentioned in Section 4.1 for the level-set function conserves only the total volume of the dispersed phase. After droplet breakup volume must be preserved for each of the two droplets. This, however, is not guaranteed with the volume conservation method currently available in DROPS. Therefore, the results presented here are of quantitative value only until 0.1 s.

5.1.3. Comparison of finite-element methods

Considering the differences between the DROPS versions discussed in Section 5.1.2, it makes sense to take a closer look at the droplet sedimentation velocities obtained using the two finite-element methods for the pressure discretization. In Fig. 10 results obtained for droplets with diameters $d = 1.0$ and 2.0 mm using the two versions are displayed, whereas all other simulation settings like time step, initial velocity and mesh size, were identical. In these plots it is noted that the XFEM technique results in sedimentation velocities that are systematically higher than those calculated by the plain DROPS version. By comparison to the

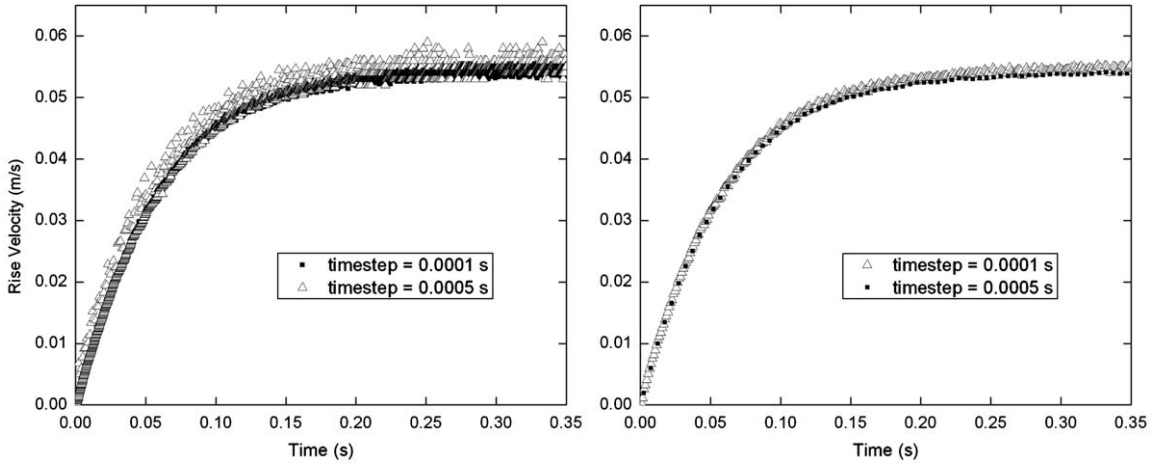

Fig. 7. Comparison of different time step sizes using XFEM-DROPS for $d = 2.0$ mm, $h = 3.13 \times 10^{-4}$ m, $h/d = 0.157$, $\xi_0 = 9.0$ mm, $v_{sed} = 0.054$ m/s. Left: raw velocity data. Right: smoothed velocity data.

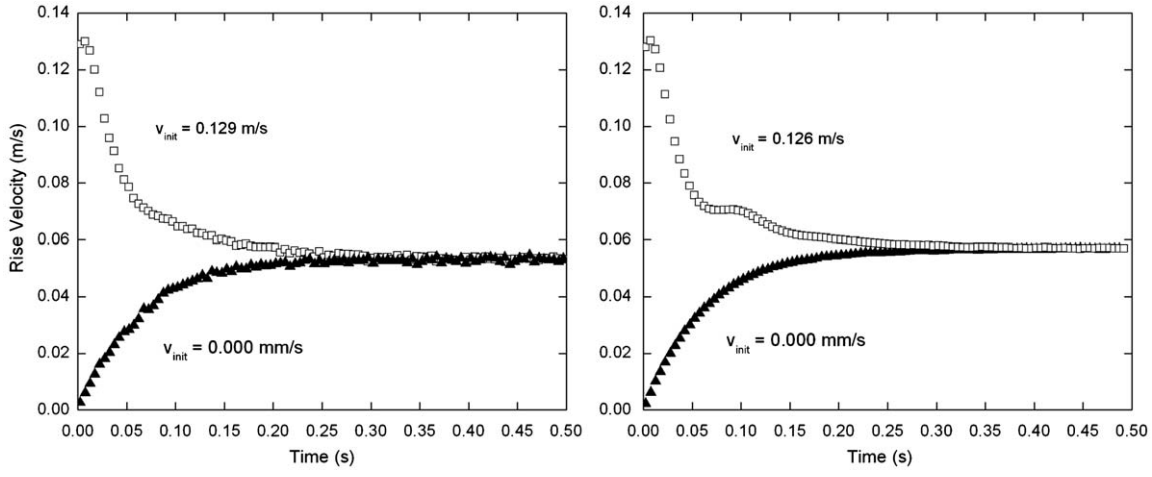

Fig. 8. Comparison of different initial conditions for $d = 2.0$ mm, $h = 3.13 \times 10^{-4}$ m, $h/d = 0.157$, $\xi_0 = 9.0$ mm. Left: plain DROPS version, $v_{sed} = 0.053$ m/s. Right: DROPS-XFEM version, $v_{sed} = 0.057$ m/s.

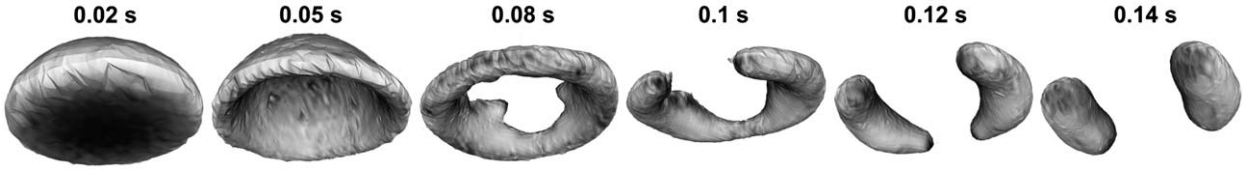

Fig. 9. Breakup stages of a droplet simulated with the plain DROPS version for $d=3.0\,\text{mm}$, $h=3.13\times10^{-4}\,\text{m}$, $h/d=0.104$, $v_{init}=0.247\,\text{m/s}$, $Re\approx500$ as seen from below when rising. The velocity is mapped on a color scale from white (for low velocities) to black (for higher velocities).

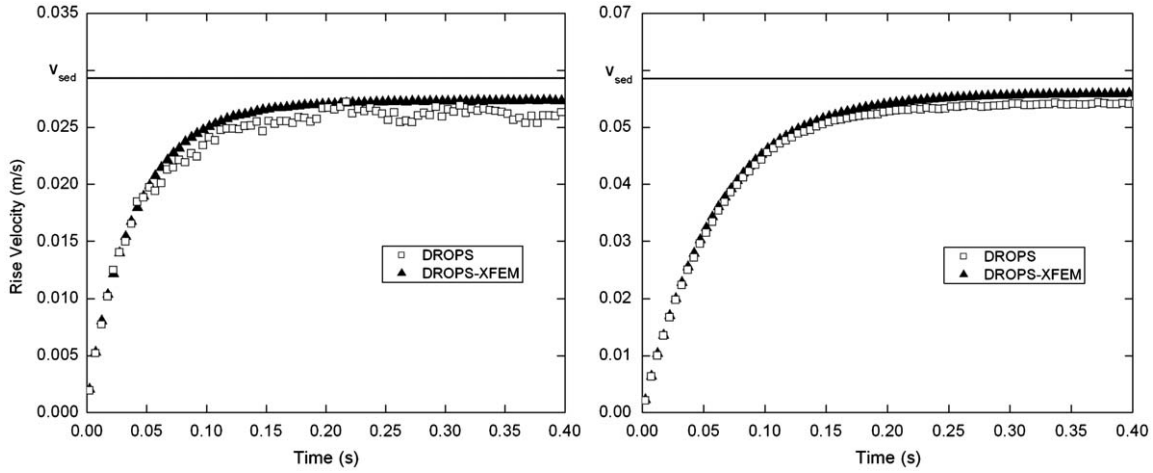

Fig. 10. Comparison between the plain DROPS version and the DROPS-XFEM version. Left: $d=1.0\,\text{mm}$, $h=1.25\times10^{-4}\,\text{m}$, $h/d=0.125$, $\xi_0=3.5\,\text{mm}$, $v_{sed}=0.027\,\text{m/s}$. Right: $d=2.0\,\text{mm}$, $h=1.56\times10^{-4}\,\text{m}$, $h/d=0.078$, $\xi_0=4.0\,\text{mm}$, $v_{sed}=0.056\,\text{m/s}$.

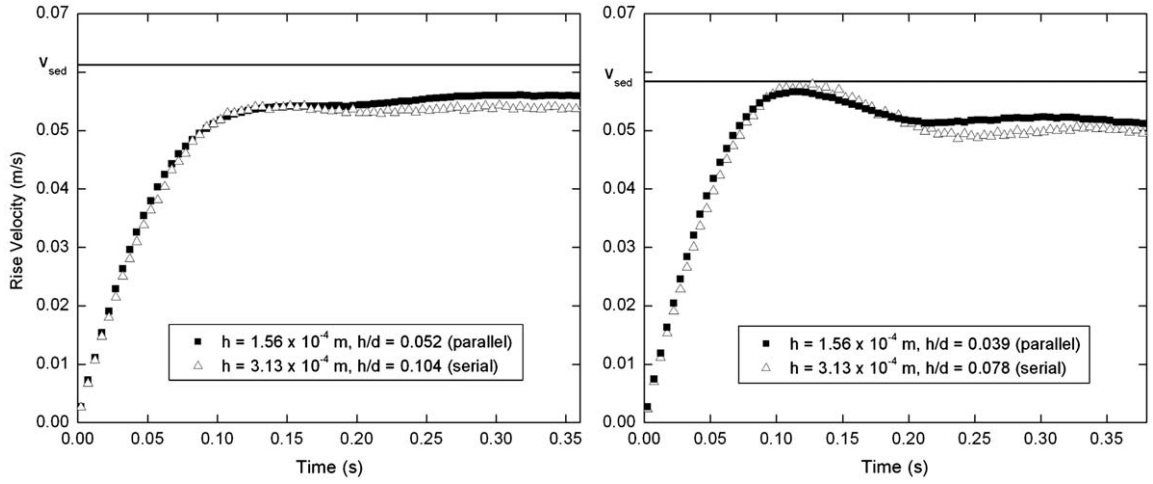

Fig. 11. Comparison of different mesh sizes for DROPS with standard FE. Left: $d=3.0\,\text{mm}$, $\xi_0=3.5\,\text{mm}$, $v_{sed}=0.056\,\text{m/s}$. Right: $d=4.0\,\text{mm}$, $\xi_0=5.0\,\text{mm}$, $v_{sed}=0.052\,\text{m/s}$.

corresponding values from the Henschke (2003) model (horizontal lines in Fig. 10) it can be concluded that the results obtained by XFEM are more accurate.

5.1.4. Grid resolution

In Fig. 11 the influence of the mesh size is presented for the DROPS version with standard finite-elements for two droplets of $d=3.0$ and $4.0\,\text{mm}$. Since the grid is configured so that the smallest mesh size is in the vicinity of the fluid interface, simulating a bigger droplet in diameter means that more of the smallest tetrahedra are necessary than in the case of a smaller droplet using the same grid configuration. For the relatively big droplets of Fig. 11 this means that the parallel DROPS version is needed in order to avoid very long calculation times. In this work, the mesh size at the droplet interface is used to represent the resolution of the grid and is denoted by h. Additionally, the dimensionless mesh size, defined by the fraction h/d, is used to indicate the grid resolution in relation to the droplet diameter. In Fig. 11 it can be seen that a finer grid results to a higher terminal droplet velocity, that is closer to the horizontal line indicating the corresponding value of the Henschke (2003) model.

In Fig. 12 the grid influence is tested for the XFEM version. In contrast to Fig. 11 it is noticed that the influence of the grid resolution is negligible between the cases studied, since a finer grid does not lead to an increase of the droplet terminal velocity. A small difference is noted only for $d=3.0\,\text{mm}$ where the terminal velocity is uninfluenced, but the two curves have a slightly different shape. Concerning the agreement of the simulations with the corresponding model we notice that the

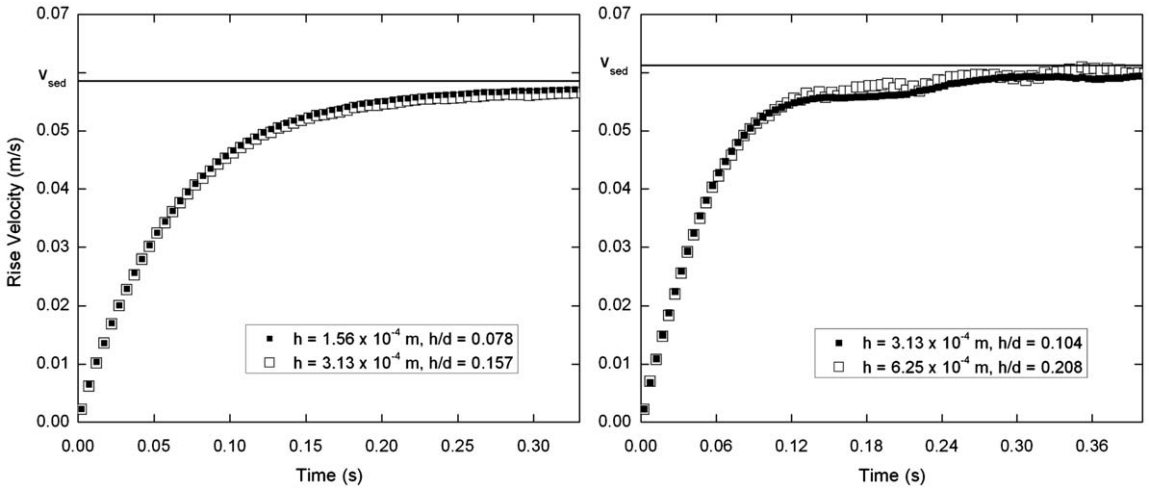

Fig. 12. Comparison of different mesh sizes for the XFEM-DROPS method. Left: $d = 2.0$ mm, $\xi_0 = 9.0$ mm, $v_{sed} = 0.057$ m/s. Right: $d = 3.0$ mm, $\xi_0 = 8.5$ mm, $v_{sed} = 0.060$ m/s.

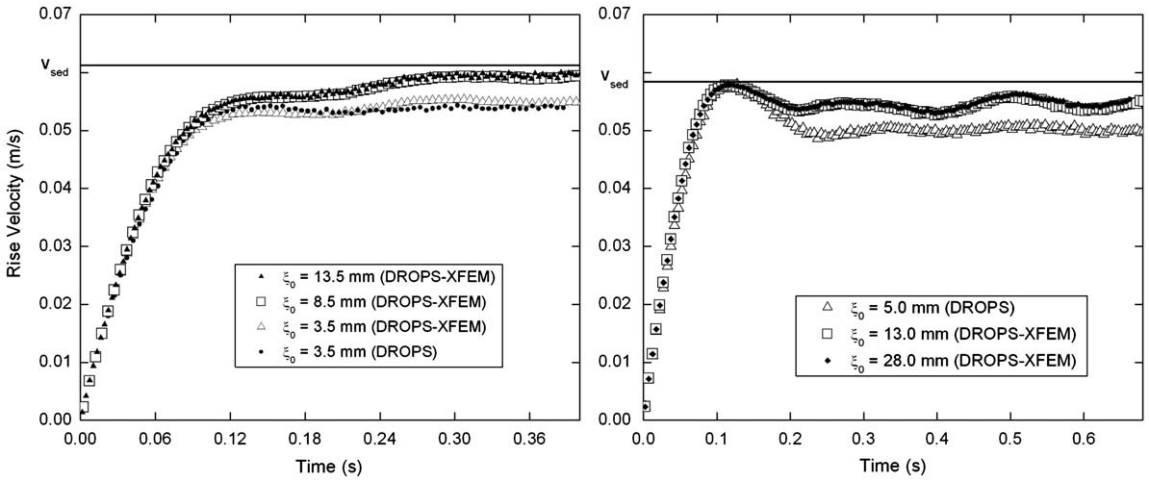

Fig. 13. Comparison of different geometry settings for $h = 3.13 \times 10^{-4}$ m. Left: $d = 3.0$ mm, $h/d = 0.104$, $v_{sed} = 0.060$ m/s. Right: $d = 4.0$ mm, $h/d = 0.078$, $v_{sed} = 0.055$ m/s.

simulations in Fig. 12 are closer to the model than the simulations in Fig. 11. This difference is not only due to the different finite-element methods but also to the size of the computational domain. This factor will be examined in Section 5.1.5.

5.1.5. *Wall effect*

Clearly, walls can have a considerable influence on the droplet sedimentation velocity (Henschke et al., 2000; Zimmerman, 2004). In this work the horizontal distance of the droplet interface to the computational domain wall at the beginning of the simulation was varied. This distance is denoted by ξ_0.

In Fig. 13 (left) a droplet with $d = 3.0$ mm is simulated using different computational domain sizes, namely, $\xi_0 = 3.5$, 8.5, and 13.5 mm. For $\xi_0 = 3.5$ mm both the XFEM-DROPS and the plain DROPS versions were tested. In agreement to the discussion in Section 5.1.3, the terminal velocity calculated by the XFEM method is higher than the one calculated by the plain method. If the droplet distance to the computational domain wall increases to $\xi_0 = 8.5$ mm, the sedimentation velocity stabilizes to an even higher value than for $\xi_0 = 3.5$ mm. A further increase of the computational domain size to $\xi_0 = 13.5$ mm does not affect the droplet velocity, thus suggesting that a safe distance of the phase interface to the wall was achieved at $\xi_0 = 8.5$ mm.

The same test was performed for a droplet diameter of $d = 4.0$ mm, and the obtained results can be seen in Fig. 13 (right). The computational domain sizes were $\xi_0 = 5.0$, 13.0, and 28.0 mm. From Fig. 13 (right) it is seen that $\xi_0 = 5.0$ mm is too small, since a rise to $\xi_0 = 13.0$ mm leads to a rise of the droplet terminal velocity. As in Fig. 13 (left) for $d = 3.0$ mm, there is also expected to be a slight influence of the choice of the finite-element method, but the wall effect is dominating in this case. A further rise to $\xi_0 = 28.5$ mm had no effect on the droplet terminal velocity or the shape of the droplet velocity curve, and therefore it is concluded that the wall-effect has been eliminated for $\xi_0 = 13.0$ mm.

Independent of the geometry configuration, a strong fluctuation occurs at the beginning of the simulation for $d = 4.0$ mm. After this initial fluctuation, the droplet reaches its terminal state. This fluctuation can also be seen in Fig. 6 where the shape of the droplet is captured at 0.2 s. Because of this fluctuation, the droplet velocity for $d = 4.0$ mm reaches a maximum, whereas for $d = 3.0$ mm the velocity rise is monotonic before the velocity plateau. In both cases in Fig. 13 velocity oscillations are noticed around a constant velocity value, although for $d = 3.0$ mm these oscillations are very weak. In such cases, this constant mean velocity is used as the droplet sedimentation velocity. As described in Section 2, such oscillations are not taken into account in the experiment, since the sedimentation velocity is measured as an average over a distance of 100 mm.

For both $d=3.0$ and 4.0 mm the computational domain size had an influence not only on the droplet terminal velocity, but also on the shape of the velocity curves of Fig. 13. More specifically, the velocity oscillations are more evident in the case of the wider computational domain. This is because the no-slip condition is applied on the computational domain boundaries, the interface is allowed to move more freely when the distance between the interface and the wall increases. Thus, the sedimentation velocity rises and the velocity oscillations get stronger. The observed oscillations for both $d=3.0$ and 4.0 mm are in accordance with the predicted diameter ranges given in Section 3 for the current system, which predict that droplets larger than 2.85 mm in diameter should oscillate.

Finally, a droplet with $d=2.0$ mm was simulated with XFEM-DROPS and two different computational domain sizes with $\xi_0=4.0$ and 9.0 mm. The influence of the computational domain wall on the droplet sedimentation velocity in this case was only 1.4%, thus setting the respective value to $v_{sed}=0.057$ m/s.

To these observations, it should be added that droplet deformation may have an impact on the extent of the wall's influence on the sedimentation velocity. If the droplet deforms to an oblate shape, as in the simulations of the present work, the interface will move closer to the wall, thus limiting its velocity. Considering a d/ξ_0 ratio instead of just ξ_0 may not necessarily resolve the issue for all liquid–liquid systems, since droplet deformation is dependent on the material properties. In the present work, $d/\xi_0=0.35$ and 0.31 were sufficient for eliminating any wall-effects for $d=3.0$ and 4.0 mm, respectively. However, it was found that the $d/\xi_0=0.35$ was marginally too high for $d=4.0$ mm. Therefore, the recommended d/ξ_0 value for the simulations discussed in this work lies between: $0.31\leq d/\xi_0<0.35$.

6. Evaluation of results

Smolianski et al. (2008) performed two-dimensional finite-element simulations of freely rising fluid particles using the level-set method and calculated the particle rise velocity as a function of time. Although fluid particles of ellipsoidal, skirted, and indented shape were also simulated, oscillations like the ones of Fig. 13, were not observed. Velocity oscillations of large fluid particles may have been suppressed by the data smoothing scheme used by Smolianski et al. (2008).

Wegener et al. (2007a) performed experiments on toluene droplets rising in water and measured their velocity as a function of time. In their work, a behavior comparable to the one presented here is shown. For relatively small droplets, the velocity rises with time until a plateau is reached where it remains constant. The duration of this smooth acceleration stage depended slightly upon the diameter of the droplet studied, but was in general not greater than 0.5 s. This observation agrees with the results of the present work if Figs. 7, 8, 10 and 12 (left) are examined, where the acceleration stage of small droplets also appears to be equally short. For bigger droplets a strong peak in the droplet velocity is noted right after the acceleration region that is very similar to the peak found in the simulations of the droplet with $d=4.0$ mm. Furthermore, after this first fluctuation, smaller oscillations around the droplet terminal velocity were also observed in the experiments of Wegener et al. (2007a), similar to the ones shown in Figs. 11 and 13.

Both Wegener et al. (2007a) and Gueyffier et al. (1999) as well as other authors like Petera and Weatherley (2001) and Wang et al. (2008) report acceleration stages that are in general no longer than 1 s in duration. These findings are also confirmed in this work.

The results presented so far provide insight as to which factors can influence the simulation results and to what extent. Parameters such as time step, initial droplet velocity, computational domain size and grid resolution have been tested. As a result these parameters can be safely set such that good accuracy in describing a sedimenting single droplet in an infinite medium is achieved while minimizing the computational effort.

In particular it is shown that for the discretization of the discontinuous pressure the extended finite element method is much better suited than the standard linear (P_1) finite-element method. In the cases of the droplets with $d=1.0$ and 2.0 mm the finest grids that were used had a smallest mesh size of $h=1.25\times10^{-4}$ and 1.56×10^{-4} m ($h/d=0.125$ and 0.078), respectively. The finest grid used for the droplets with $d=3.0$ and 4.0 mm had a smallest mesh size of $h=3.13\times10^{-4}$ m ($h/d=0.104$ and 0.078). The distance to the wall was set according to the discussion in Section 5.1.5. The size of the timestep that was used was equal to 5.0×10^{-4} s, as discussed in Section 5.1.1. The final results of simulations performed with the above specifications are presented in Fig. 14 together with the line of Fig. 2 for representing the droplets with an ideally mobile interface.

In Fig. 14 the model curve of Section 3 for an ideally mobile interface is compared to the DROPS-XFEM results. Since in the simulations no interfacial stagnation is considered, the simulation results are compared to the model curve that also makes the same assumption, i.e. that the interface is ideally mobile. In the figure, it can be seen that the results of the simulations are in good quantitative agreement with the model curve. The experiments, and consequently the fitted model, suggest a rise of the terminal velocity with increasing droplet diameter that subsequently reaches a maximum and then decays. These three curve characteristics as well as their corresponding locations on the diagram are all well-predicted by the simulations.

The model curve is extended only up to the maximum droplet diameter that has been investigated in the experiments ($d=3.48$ mm). Extrapolating the model curve beyond that point would not necessarily depict the experimental data trend, since only two experimental points are in the oscillating droplet region. The experimental data in this region influence the fitting of the model parameter p_2, that determines the vertical position of the plateau of the sedimentation curve for oscillating droplets. After considering these facts, it can be stated that the result of the DROPS-XFEM simulation for $d=4.0$ mm fits nicely to the experimental data in the oscillating region, and is in agreement with their trend. The simulation results are included in the data summary given in Table 2.

7. Conclusions and future work

In this paper simulations of single *n*-butanol droplets rising in water were presented. The simulation techniques implemented in this work were validated with the help of experimental results and empirical models in terms of both numerical and physical aspects.

The finite-element and the extended finite-element techniques were tested in the solver and the level-set method was implemented for capturing the ideally movable interface. The continuum surface-force model was used to take surface-tension effects into account. The instationary simulations were performed with a fixed three-dimensional coordinate system and a hierarchy of tetrahedral grids, locally refined close to the interface. The grid is dynamically adjusted in the course of the simulation to follow the movement of the interface.

The droplet diameters that were studied spanned the regions of spherical, deformed, and oscillating droplets, thus testing the

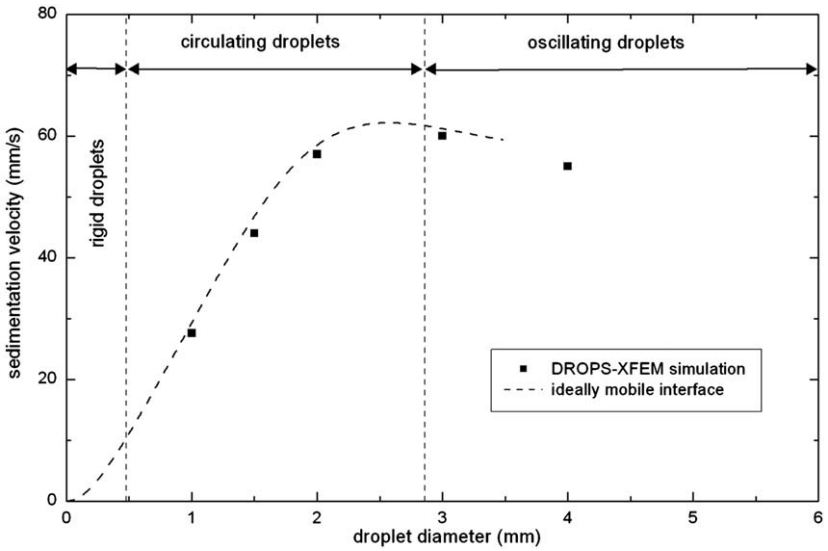

Fig. 14. Comparison of simulation results to model curve for an ideally mobile interface.

numerical techniques under very different conditions that are technically relevant to the liquid–liquid extraction systems. The simulations included the stages of drop acceleration, deformation, and stability in terms of shape and velocity. Droplet breakup of large droplets was also simulated. The results show that these techniques provide a solid computational basis that delivers results in agreement with existing semi-empirical models and experimental data. Simulation parameters like mesh size, time-step, computational domain size, and droplet initial velocity have been tested in order to produce more realistic results. The extended finite-element method was found to be superior to the standard finite-element method, thus making it the preferred technique for the simulation of droplets in technical liquid–liquid systems.

It is concluded that the DROPS simulation tool is reliable for simulating the behavior of buoyancy-driven droplets. The results provide the motivation to extend the capabilities of the solver to take into account mass transfer of a third component through the interface, as well as inhomogeneities of the surface tension, typically induced by surfactant impurities in the system.

Notation

Ar	Archimedes number
C_D	drag coefficient
d	droplet diameter
Eo	Eötvös number
f	correction term for Hadamard–Rybczynski factor
f'	rigid to circulating droplet transition factor
f_Γ	surface force
g	gravitational acceleration
h	smallest mesh element size
H	Heaviside function
$\mathbf{I}$	identity matrix
$\mathcal{I}_\Gamma$	indices of tetrahedra intersected by the interface
K_{HR}	Hadamard–Rybczynski factor
K'_{HR}	corrected Hadamard–Rybczynski factor
Mo	Morton number
$\mathbf{n}$	unit normal at the interface
p	pressure
q_i	nodal basis functions
q_i^Γ	additional basis functions of XFEM space
Q_h	standard finite element space
Q_h^Γ	extended finite element space
Re	Reynolds number
t	time
$\mathbf{u}$	velocity vector
v_{init}	droplet velocity at initial simulation time step
v_{sed}	droplet sedimentation velocity
x	space

Greek letters

Γ	interfacial surface
δ_Γ	Dirac δ- function with support on Γ
κ	curvature of interfacial surface
μ	dynamic viscosity
ξ_0	horizontal distance of droplet interface to computational domain wall at the simulation beginning
ρ	density
$\Delta\rho$	absolute density difference between continuous and dispersed phase
$\boldsymbol{\sigma}$	stress tensor
σ	interfacial tension
ϕ	level-set function
Ω_1	droplet domain
Ω_2	continuous phase domain

Subscripts

c	property of continuous phase
$circ$	property of droplet with internal circulation
d	property of dispersed phase
def	property of deformed droplet
os	property of oscillating droplet
$rigid$	property of droplet with no internal circulation
$sphere$	property of spherical droplet

Acknowledgment

This project was funded by the German Research Foundation (DFG) in the framework of the collaborative research centre CRC

540 "Model-based Experimental Analysis of Kinetic Phenomena in Fluid Multi-phase Reactive Systems".

References

Alves, S.S., Orvalho, S.P., Vasconcelos, J.M.T., 2005. Effect of bubble contamination on rise velocity and mass transfer. Chemical Engineering Science 60, 1–9.

Brackbill, J.U., Kothe, D.B., Zemach, C., 1992. A continuum method for modelling surface tension. Journal of Computational Physics 100, 335–354.

Brauer, H., 1973. Impuls-, Stoff-, und Wärmetransport durch die Grenzfläche kugelförmiger Partikeln. Chemie Ingenieur Technik 45 (18), 1099–1103.

Bristeau, M.O., Glowinski, R., Periaux, J., 1987. Numerical methods for the Navier–Stokes equations applications to the simulation of compressible and incompressible viscous flows. Computer Physics Reports 6, 73–187.

Chang, Y.C., Hou, T.Y., Merriman, B., Osher, S., 1996. A level set formulation of Eulerian interface capturing methods for incompressible fluid flows. Journal of Computational Physics 124, 449–464.

Clift, R., Grace, J.R., Weber, M.E., 1978. Bubbles, Drops, and Particles. Academic Press, London.

Cristini, V., Blawzdziewicz, J., Lowenberg, M., 1998. Drop breakup in three-dimensional viscous flows. Physics of Fluids 10 (8), 1781–1783 (letter).

Cristini, V., Blawzdziewicz, J., Lowenberg, M., 2001. An adaptive mesh algorithm for evolving surfaces: simulations of drop breakup and coalescence. Journal of Computational Physics 168, 445–463.

Dehkordi, A.M., Ghasemian, S., Bastani, D., Ahmadpour, N., 2007. Model for excess mass-transfer resistance of contaminated liquid–liquid systems. Industrial and Engineering Chemistry Research 46, 1563–1571.

Deshpande, K.B., Zimmerman, W.B., 2006. Simulations of mass transfer limited reaction in a moving droplet to study transport limited characteristics. Chemical Engineering Science 61, 6424–6441.

Feigl, K., Megias-Alguacil, D., Fischer, P., Windhab, E.J., 2007. Simulation and experiments of droplet deformation and orientation in simple shear flow with surfactants. Chemical Engineering Science 62, 3242–3258.

Gross, S., Peters, J., Reichelt, V., Reusken, A., 2002. The DROPS package for numerical simulations of incompressible flows using parallel adaptive multigrid techniques. Preprint 227, RWTH Aachen.

Gross, S., Reichelt, V., Reusken, A., 2006. A finite element based level set method for two-phase incompressible flows. Computing and Visualization in Science 9 (4), 239–257.

Gross, S., Reusken, A., 2005. Parallel multilevel tetrahedral grid refinement. SIAM Journal on Scientific Computing 26 (4), 1261–1288.

Gross, S., Reusken, A., 2007a. An extended pressure finite element space for two-phase incompressible flows with surface tension. Journal of Computational Physics 224, 40–58.

Gross, S., Reusken, A., 2007b. Finite element discretization error analysis of a surface tension force in two-phase incompressible flows. SIAM Journal on Numerical Analysis 45 (4), 1679–1700.

Gross, S., Soemers, M., Mhamdi, A., Al-Sibai, F., Reusken, A., Marquardt, W., Renz, U., 2005. Identification of boundary heat fluxes in a falling film experiment using high resolution temperature measurements. International Journal of Heat and Mass Transfer 48, 5549–5562.

Gross-Hardt, E., Henschke, M., Klinger, S., Pfennig, A., 2002. Design of pulsed extraction columns based on lab-scale experiments with a small number of drops. In: Sole, K.C., Cole, P.M., Preston, J.S., Robinson, D.J. (Eds.), International Solvent Extraction Conference (ISEC). South African Institute of Mining and Metallurgy, Johannesburg, pp. 1358–1363.

Gueyffier, D., Li, J., Nadim, A., Scerdovelli, R., Zaleski, S., 1999. Volume-of-fluid interface tracking with smoothed surface stress methods for three-dimensional flows. Journal of Computational Physics 152, 426–456.

Haas, U., Schmidt-Traub, H., Brauer, H., 1972. Umströmung kugelförmiger Blasen mit innerer Zirkulation. Chemie Ingenieur Technik 44 (18), 1060–1068.

Hansbo, A., Hansbo, P., 2004. A finite element method for the simulation of strong and weak discontinuities in solid mechanics. Computer Methods in Applied Mechanics and Engineering 193 (33–35), 3523–3540.

Hendrix, C.D., Dave, S.B., Johnson, H.F., 1967. Translation of continuous phase in the wakes of single rising drops. American Institute of Chemical Engineers Journal 13 (6), 1072–1077.

Henschke, M., 2003. Auslegung pulsierter Siebboden-Extraktionskolonnen. Shaker Verlag, Aachen.

Henschke, M., Pfennig, A., 1999. Mass-transfer enhancement in single drop extraction experiments. American Institute of Chemical Engineers Journal 45 (10), 2079–2086.

Henschke, M., Waheed, A., Pfennig, A., 2000. Wandeinfluss auf die Sedimentationsgeschwindigkeit von Kugeln. Chemie Ingenieur Technik 72 (11), 1376–13801.

Hirt, C.W., Nichols, B.D., 1981. Volume of fluid (VOF) method for the dynamics of free boundaries. Journal of Computational Physics 39, 201–225.

Hu, S., Kintner, R.C., 1955. The fall of single liquid drops through water. American Institute of Chemical Engineers Journal 1 (1), 42–48.

Kalem, M., Pfennig, A., 2007. ReDrop—a general method for solving drop-population balances with an arbitrary number of property variables. In: Plesu, V., Agachi, P.S. (Eds.), 17th European Symposium on Computer Aided Process Design—ESCAPE17.

Koebe, M., 2004. Numerische Simulation aufsteigender Blasen mit und ohne Stoffaustausch mittels der Volume of Fluid (VOF) Methode. Ph.D. Thesis, Fakultät für Maschinenbau, Universität Paderbon.

Koh, C.J., Leal, L.G., 1990. An experimental investigation on the stability of viscous drops translating through a quiescent fluid. Physics of Fluids A 2 (12), 2103–2109.

Levich, V.G., 1962. Physicochemical Thermodynamics. Prentice-Hall, New Jersey.

Li, X.-J., Mao, Z.-S., 2001. The effect of surfactant on the motion of a buoyancy-driven drop at intermediate Reynolds numbers: a numerical approach. Journal of Colloid and Interface Science 240, 307–322.

Li, X.-J., Mao, Z.-S., Fei, W., 2003. Effects of surface-active agents on mass transfer of a solute into single buoyancy driven drops in solvent extraction systems. Chemical Engineering Science 58, 3793–3806.

Mack, C., 2001. Untersuchungen zum Stofftransport von Chrom(III) und Zink(II) bei der Extraction mittels Bis(2-ethylhexyl)-phosphorsäure. Ph.D. Thesis, Technischen Universität Darmstadt, Darmstadt.

Maneri, C.C., 1995. New look at wave analogy for prediction of bubble terminal velocities. American Institute of Chemical Engineers Journal 41 (3), 481–487.

Mao, Z.-S., Li, T., Chen, J., 2001. Numerical simulation of steady and transient mass transfer to single drop dominated by external resistance. International Journal of Heat and Mass Transfer 44, 1235–1247.

Mekasut, L., Molinier, J., Angelino, H., 1979. Effects of surface-active agents on mass transfer inside drops. Chemical Engineering Science 34, 217–224.

Misek, T., Berger, R., Schröter, J., 1985. Standard test systems for liquid extraction. In: European Federation of Chemical Engineering Publications Series, no. 46, second ed. Institution of Chemical Engineers, Warwickshire.

Modigell, M., 1981. Untersuchung der Stoffübertragung zwischen zwei Füssigkeiten unter Berücksichtigung von Grenzflächenphänomenen. Ph.D. Thesis, RWTH-Aachen University.

Moës, N., Dolbow, J., Belytschko, T., 1999. A finite element method for crack growth without remeshing. International Journal for Numerical Methods in Engineering 46, 131–150.

Muradoglu, M., Tryggvason, G., 2008. A front-tracking method for computation of interfacial flows with soluble surfactants. Journal of Computational Physics 227, 2238–3362.

Noh, D.S., Kang, I.S., Leal, L.G., 1993. Numerical solutions for the deformation of a bubble rising in dilute polymeric fluids. Physics of Fluids A 5 (6), 1315–1332.

Osher, S., Sethian, J., 1988. Fronts propagating with curvature-dependent speed: algorithms based on Hamilton–Jacobi formulations. Journal of Computational Physics 79, 12–49.

Paesch, T., 1998. Untersuchung und Bewertung des Stoffaustauschverhaltens von Einzeltropfen unter Berücksichtigung fluiddynamischer und thermodynamischer Parameter. Master's Thesis, Lehrstuhl für Thermische Verfahrenstechnik, RWTH Aachen.

Patel, P.D., Shaqfeh, E.S., Butler, J.E., Cristini, V., Blawzdziewicz, J., Lowenberg, M., 2003. Drop breakup in the flow through fixed fiber beds: an experimental and computational investigation. Physics of Fluids 15 (5), 1146–1157.

Petera, J., Weatherley, L.R., 2001. Modelling of mass transfer from falling droplets. Chemical Engineering Science 56, 4929–4947.

Pillapakkam, S.B., Singh, P., 2001. A level-set method for computing solutions to viscoelastic two-phase flow. Journal of Computational Physics 174, 552–578.

Quan, S., Schmidt, D.P., 2006. Direct numerical study of a liquid droplet impulsively accelerated by gaseous flow. Physics of Fluids 18, 102103.

Renardy, Y.Y., Renardy, M., Cristini, V., 2001. A new volume-of-fluid formulation for surfactants and simulations of drop deformation under shear at a low viscosity ratio. European Journal of Mechanics. B. Fluids 21, 49–59.

Reusken, A., 2008. Analysis of an extended pressure finite element space for two-phase incompressible flows. Computing and Visualization in Science 11, 293–305.

Reusken, A., et al., 2009. DROPS internet homepage and manual 〈http://www.igpm.rwth-aachen.de/drops〉.

Roos, H.-G., Stynes, M., Tobiska, L., 1996. Numerical methods for singularly perturbed differential equations. In: Springer Series in Computational Mathematics, vol. 24. Springer, Berlin.

Rose, P.M., Kintner, R.C., 1966. Mass transfer from large oscillating drops. American Institute of Chemical Engineers Journal 12 (3), 530–534.

Ryskin, G., Leal, L.G., 1983. Orthogonal mapping. Journal of Computational Physics 50, 71–100.

Smolianski, A., 2005. Finite-element/level-set/operator-splitting (FELSOS) approach for computing two-fluid unsteady flows with free moving interfaces. International Journal of Numerical Methods in Fluids 48 (3), 231–269.

Smolianski, A., Haario, H., Luukka, P., 2008. Numerical study of dynamics of single bubbles and bubble swarms. Applied Mathematical Modelling 32 (5), 641–659.

Steiner, L., Oezdemir, G., Hartland, S., 1990. Single-drop mass transfer in the water-toluene-acetone system. Industrial and Engineering Chemistry Research 29, 1313–1318.

Sussman, M., Smereka, P., Osher, S., 1994. A level set approach for computing solutions to incompressible two-phase flow. Journal of Computational Physics 114, 146–159.

Sussman, M., Almgren, A.S., Bell, J.B., Colella, P., Howell, L.H., Welcome, M.L., 1999. An adaptive level set approach for incompressible two-phase flows. Journal of Computational Physics 148, 81–124.

Sussman, M., Smith, K.M., Hussaini, M.Y., Ohta, M., Zhi-Wei, R., 2007. A sharp interface method for incompressible two-phase flows. Journal of Computational Physics 221, 469–505.

Terboven, C., Spiegel, A., an Mey, D., Gross, S., Reichelt, V., 2005. Experiences with the OpenMP parallelization of DROPS, a Navier–Stokes solver written in C++. In: First International Workshop on OpenMP (IWOMP), Oregon, USA, published electronically.

Tornberg, A.-K., Engquist, B., 2000. A finite element based level-set method for multiphase flow applications. Computing and Visualization in Science 3, 93–101.

Tryggvason, G., Bunner, B., Esmaeeli, A., Juric, D., Al-Rawahi, N., Tauber, W., Han, J., Nas, S., Jan, Y.-J., 2001. A front tracking method for the computations of multiphase flow. Journal of Computational Physics 169, 708–759.

Waheed, M.A., 2001. Fluiddynamik und Stoffaustausch bei freier und erzwungener Konvektion umströmter Tropfen. Ph.D. Thesis, Lehrstuhl für Thermische Verfahrenstechnik, RWTH-Aachen University.

Waheed, M.A., Henschke, M., Pfennig, A., 2004. Simulating sedimentation of liquid drops. International Journal for Numerical Methods in Engineering 59, 1821–1837.

Walker, D.W., Dongarra, J.J., 1996. MPI: a standard message passing interface. Supercomputer 12 (1), 56–68.

Wang, T., Wang, J., 2007. Numerical simulations of gas-liquid mass transfer of gas–liquid mass transfer in bubble columns with a CFD-PBM coupled model. Chemical Engineering Science 62, 7107–7118.

Wang, J., Lu, P., Wang, Z., Yang, C., Mao, Z.-S., 2008. Numerical simulation of unsteady mass transfer by the level set method. Chemical Engineering Science 63, 3141–3151.

Wegener, M., Grünig, J., Stüber, J., Paschedag, A.R., Kraume, M., 2007a. Transient rise velocity and mass transfer of a single drop with interfacial instabilities —experimental investigations. Chemical Engineering Science 62, 2967–2978.

Wegener, M., Paschedag, A.R., Kraume, M., 2007b. Experimentelle Untersuchungen sowie 2D- und 3D-Simulationen zum Stofftransport an Einzeltropfen mit Marangoni-Konvektion. Chemie Ingenieur Technik 79, 73–81.

Yang, C., Mao, Z.-S., 2005. Numerical simulation of interphase mass transfer with the level set approach. Chemical Engineering Science 60, 2643–2660.

Yang, X., James, A.J., Lowengrub, J., Zheng, X., Cristini, V., 2006. An adaptive coupled level-set/volume-of-fluid interface capturing method for unstructured triangular grids. Journal of Computational Physics 217, 364–394.

Zimmerman, W.B., 2004. On the resistance of a spherical particle settling in a tube of viscous fluid. International Journal of Engineering Science 42, 1753–1778.

Zimmerman, W.B.J., 2006. Multiphysics modelling with finite element methods. In: Series on Stability, Vibration and Control of Systems (A), vol. 18. World Scientific, London (Modeling of multi-phase flow using the level set method, pp. 277–299, Chapter 8).